

BENDING PROPERTIES OF COMPOSITE SLAB DEVELOPED ON RECTANGULAR-FINNEED BASE SLABS

BIN LUO, WEI HUANG *

College of Civil Engineering, Xi'an University of Architecture & Technology, Xi'an 710055, China

This paper aims to disclose the bending properties of composite slab and base slab made from recycled concrete. For this purpose, our research group created haydites from underground sludge and discarded bricks, and mixed them with steel fibres into steel fibre-reinforced recycled haydite concrete (Concrete A) and steel fibre-reinforced recycled brick concrete (Concrete B). Then, each of the two recycled concretes was casted into a rectangular-finned prefabricated (RFP) base slab, which is known for its excellent rigidity, strong bearing capacity and large contact area. For comparison, another RFP base slab was made from ordinary concrete. After that, ordinary concrete was poured onto the three RFP base slabs, forming three composite slabs. Next, static load tests were performed on full-size specimens on all three RFP base slabs and three composite slabs. Based on the test results, the failure features of the specimens and the synergic effect between old and new concretes were discussed in light of the load-deflection curves, load-bar strain curves, contact area between base slab and upper-layer concrete, load-compressive strain curves and feature parameters. It is concluded that under static vertical load, the base slabs and composite slabs made from recycled concretes shared the same failure process with those made from ordinary concretes; the old and new concretes exhibited excellent bonding and synergic effects; the base plate made from Concrete B boasted the highest bearing capacity and lowest deflection among all base plates and composite plates investigated in our research. The research findings lay a solid basis for the research and application of recycled concrete composite slabs.

Keywords: Recycled aggregates; Bending properties; Rectangular-finned prefabricated (RFP) base slab

1. Introduction

With the development of construction industry, there has been an upsurge in the amount of construction wastes. This trend not only precludes environmental pollution, but also signifies resource wasting. To solve the problems, it is necessary to replace natural aggregates with recycled ones produced from construction wastes. The recycled aggregates, as an environmental-friendly and resource-saving material, enjoy a great potential of application [1, 2]. One of the potential application areas is the manufacturing of composite slabs. Composite slab is an important component of prefabricated concrete structure. As its name suggests, composite slab encompasses both prefabricated and cast-in-situ parts. The slab is usually produced in two phases: first, hoist the prefabricated base slab to the right position; then, pour concrete onto the base slab, such that the upper-layer concrete form an integrated whole with the base slab. In this way, the two parts can bear the loads on the composite slab together. Over the years, composite slabs have been widely used in engineering, because of their favourable impacts like automatic production, assembly operation, resource efficiency and fast construction [3-7].

In light of the above, our research group created haydites from underground sludge and

discarded bricks, and mixed them with steel fibres into steel fibre-reinforced recycled haydite concrete (Concrete A) and steel fibre-reinforced recycled brick concrete (Concrete B) [8,9]. Then, each of the two recycled concretes was casted into a rectangular-finned prefabricated (RFP) base slab, which is known for its excellent rigidity, strong bearing capacity and large contact area [10-12]. For comparison, another RFP base slab was made from ordinary concrete. After that, ordinary concrete was poured onto the three RFP base slabs, forming three composite slabs. Next, static load tests were performed on full-size specimens on all three RFP base slabs and three composite slabs, aiming to compare the bending properties between the proposed base slabs/composite slabs and the contrast base slab/composite slab and disclose the synergistic effect between the recycled concrete in the base slab and the ordinary concrete in the upper layer. The research findings lay a solid basis for the research and application of recycled concrete composite slabs.

2. Methodology

2.1. Specimen design

A total of 6 one-way slab specimens were designed, including 3 RFP base slabs and 3 composite slabs. Each slab is 3,000mm long, with

* Autor corespondent/Corresponding author,
E-mail: Robin198595@163.com

Table 1

| No. | RFP base slab | | | | Upper-layer concrete | Base slab length*base slab width*base slab thickness*upper-layer thickness (mm) |
|-------|-------------------|---------------|-------------------|----------------|-----------------------|---|
| | Material | Fibre content | Replacement ratio | Strength grade | | |
| DHB-1 | Ordinary concrete | — | — | C30 | C30 ordinary concrete | 3000*900*60*60 |
| DHB-2 | Concrete A | 1% | 100% | C30 | C30 ordinary concrete | 3000*900*60*60 |
| DHB-3 | Concrete B | 1% | 100% | C30 | C30 ordinary concrete | 3000*900*60*60 |
| YDB-1 | Ordinary concrete | — | — | C30 | — | 3000*900*60*60 |
| YDB-2 | Concrete A | 1% | 100% | C30 | — | 3000*900*60*60 |
| YDB-3 | Concrete B | 1% | 100% | C30 | — | 3000*900*60*60 |

Note: 1. For each specimen, the contact area between the bottom slab and the upper-layer concrete was roughened to ensure that the convex-concave degree is greater than 4mm; 2. YDB stands for RFP base slab specimen and DHB refers to composite slab specimen; 3. Replacement ratio means the ratio of traditional coarse aggregates being replaced by recycled coarse aggregates.

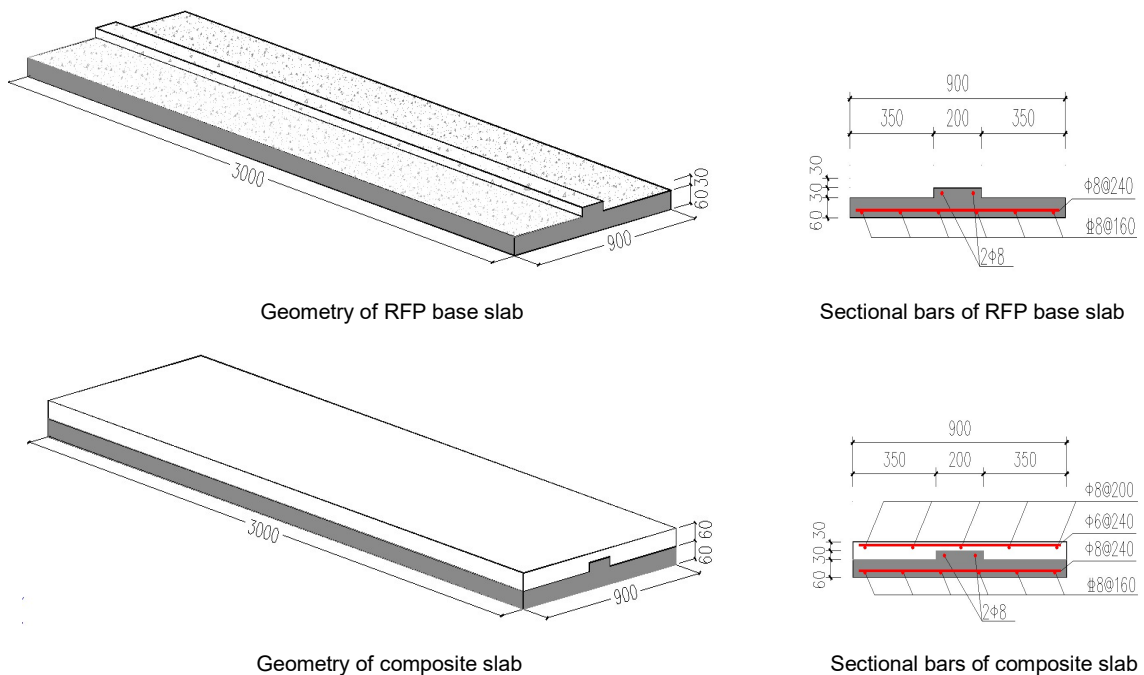


Fig. 1 - The structure and bars of the specimens

an effective length of 2,840mm. The three RFP base slabs were respectively made from ordinary concrete, Concrete A and Concrete B; the upper layers of all three composite slabs were made from ordinary concrete. The codes and parameters of these specimens are listed in Table 1. Each base slab was reinforced by C8@160 longitudinal load-bearing bars and $\Phi 8@240$ transversely distributed bars, while each upper-layer concrete was reinforced by $\Phi 8@200$ longitudinal load-bearing bars and $\Phi 6@240$ transversely distributed bars. To prevent the base slabs from cracking in hoisting, 2 $\Phi 8$ bars were added to the rectangular fins of each RFP base slab. The structure and bars of the specimens are illustrated in Figure 1.

2.2. Physical-mechanical properties of materials

For Concrete A, the coarse aggregates and

fine aggregates were produced from underground sludge and natural sand, respectively; the replacement ratio, steel fibre content and designed strength are 100%, 1% and C30, respectively. For Concrete B, the coarse aggregates and fine aggregates were produced from abandoned bricks and natural sand, respectively; the replacement ratio, steel fibre content and designed strength were the same with those of Concrete A.

According to the Code for Design of Concrete Structures (GB50010-2010 (2016)), a cubic block (150mm×150mm×150mm) and a prismatic block (150mm×150mm×150mm) were created for each specimen, and subjected to the static load tests after 28 days of standard curing. The results of both blocks were averaged and recorded as the concrete strength (Table 2).

Table 2

| Mechanical properties of concretes | | | | | |
|------------------------------------|--|---------------------------------------|---------------------------------|----------------------------|-----------------------|
| Material | Cubic compressive strength f_{cu} /MPa | Axial compressive strength f_c /MPa | Tensile strength $f_{t,s}$ /MPa | Elastic modulus E_c /MPa | Poisson's ratio μ |
| Ordinary concrete | 33.9 | 25.7 | 4.04 | 3.20×10^4 | 0.2 |
| Concrete A | 32.4 | 21.7 | 3.89 | 3.06×10^4 | 0.2 |
| Concrete B | 43.0 | 32.7 | 4.21 | 3.32×10^4 | 0.2 |

Table 3

| Mechanical properties of bars | | | |
|-------------------------------|----------------------|-------------------------|-----------------------|
| Diameter / mm | Yield strength / MPa | Ultimate strength / MPa | Elastic Modulus / MPa |
| Φ6 | 300 | 429 | 2.1×10^5 |
| Φ8 | 310 | 447 | 2.1×10^5 |
| D8 | 434 | 613 | 2.0×10^5 |

Note: The Φ6 bar is the transversely distributed bar of each RFP base slab; the first D8 bar is the longitudinal load-bearing bar of each base slab; the second Φ8 bar is the transversely distributed bar in the upper-layer concrete.

The longitudinal load-bearing bars in each base slab were of the grade HRB400, and all the other bars in the specimens were of the grade HPB300. The mechanical properties of these bars are displayed in Table 3. Corrugated steel fibres were applied to the RFP base slabs. The length, diameter, tensile strength and elastic modulus of the fibres were 35mm, 0.56mm, 2.3×10^4 MPa and 2×10^4 MPa, respectively.

2.3. Loading plan

Two equal vertical loads were applied evenly by jack and distributive girder onto the quarter span points of each composite slab, and measured with a load sensor.

The loading process was divided into several phases based on the ultimate strength and the maximum service load calculated for one-way slabs.

In our test, the maximum service load refers to the load under which the midspan deflection of the specimen reaches 1/200 of the span or the maximum crack width exceeds 0.20mm; the ultimate strength was assumed to occur in one of the following conditions: the midspan deflection of the specimen reaches 1/50 of the span, the crack width of the main tensile bar widens to 1.50mm, the bar strain became 0.01, and the tensile bar broke due to the concrete failure in the compressive zone [13].



Fig. 2 - Test Loading Test Site

The pre-loading phase includes three loading stages and three unloading stages. The load increment of each stage was 2kN. In the formal

loading phase, the load increment was initially kept at 2kN per stage, adjusted to 4kN per stage after the emergence of cracks on the concrete, and changed back to 2kN per stage when the load reached 90% of the calculated ultimate strength. The load was maintained for 5~10min after the loading/unloading at each stage. The data were not read before the instruments became stable. The secondary stress on composite slabs was neglected. The loading plan for composite slabs was also applied to the loading of RFP base slabs, except that the load per stage is half the value for composite slabs.

2.4. Arrangement of measuring points

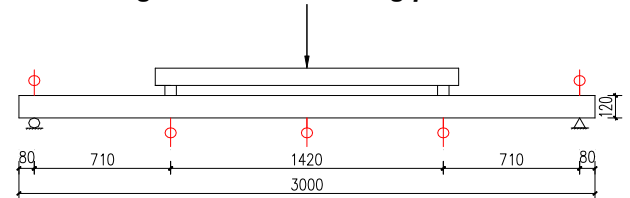


Fig. 3 - Loading plan and measuring points

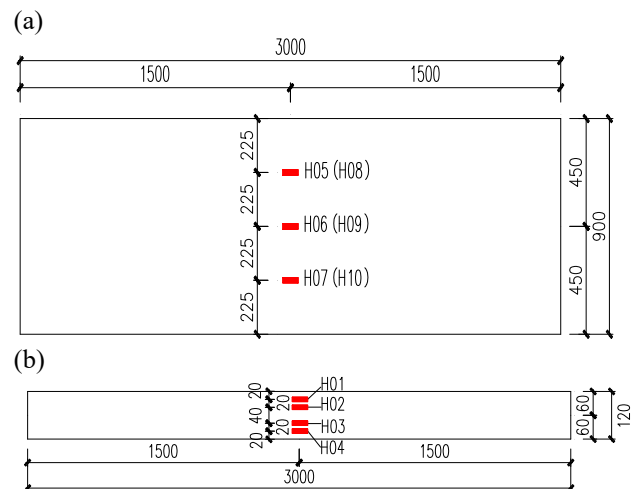


Fig. 4 - Measuring points on the concrete: (a) Top view; (b) Side view

The load sensor was arranged between a vertical jack and a simply supported steel beam. The deflection measuring points were arranged at midspan and quarter span points, as well as the support to observe deformation of the specimen (Figure 3). The bar strain gages were pasted at midspan and quarter span points of longitudinal tensile bars at the bottom to observe the stress development of the bars. Moreover, strain gages were arranged on the upper surface, lower surface and sides of the concrete in composite slab specimens (Figure 4).

3. Test results and Analysis

3.1. Test process and failure features

Throughout the tests, the six specimens all went through three obvious phases, namely, the elastic phase, the elastic-plastic phase and the failure phase. Moreover, the final failures all carried the typical features of bending failure. The specimens displayed good deformation performance, as evidenced by the wide propagation of cracks, even and dense distribution of cracks and the large damage and yield deflections. However, the specimens differed slightly in properties across the test phases, for the RFP slabs are made from different concretes. The ultimate failure patterns of composite slab specimens and RFP slab specimens are shown in Figure 5 and Figure 6, respectively.



a) DHB-1 bottom crack

| | | | | | | | | | | | | | | | | | | | |
|----|------|----|----|----|----|----|----|----|----|----|----|----|----|----|----|----|----|----|----|
| 6 | 7 | 8 | 9 | 10 | 11 | 12 | 13 | 14 | 15 | 16 | 17 | 18 | 19 | 20 | 21 | 22 | 23 | 24 | 25 |
| 34 | 57.8 | 52 | 52 | 52 | 54 | 54 | 54 | 54 | 54 | 54 | 54 | 54 | 54 | 54 | 54 | 54 | 54 | 54 | 54 |

b) DHB-1 side crack



c) DHB-2 bottom crack

| | | | | | | | | | | | | | | | | | | | |
|----|----|----|----|----|----|----|----|----|----|----|----|----|----|----|----|----|----|----|----|
| 6 | 7 | 8 | 9 | 10 | 11 | 12 | 13 | 14 | 15 | 16 | 17 | 18 | 19 | 20 | 21 | 22 | 23 | 24 | 25 |
| 43 | 58 | 58 | 58 | 58 | 58 | 58 | 58 | 58 | 58 | 58 | 58 | 58 | 58 | 58 | 58 | 58 | 58 | 58 | 58 |

d) DHB-2 side crack



e) DHB-3 bottom crack

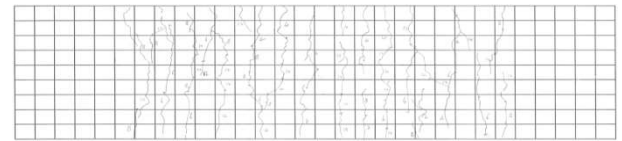
| | | | | | | | | | | | | | | | | | | | |
|----|----|----|----|----|----|----|----|----|----|----|----|----|----|----|----|----|----|----|----|
| 6 | 7 | 8 | 9 | 10 | 11 | 12 | 13 | 14 | 15 | 16 | 17 | 18 | 19 | 20 | 21 | 22 | 23 | 24 | 25 |
| 43 | 48 | 48 | 48 | 48 | 48 | 48 | 48 | 48 | 48 | 48 | 48 | 48 | 48 | 48 | 48 | 48 | 48 | 48 | 48 |

f) DHB-3 side crack

Fig. 5 - Ultimate Failure pattern of Composite Slab.



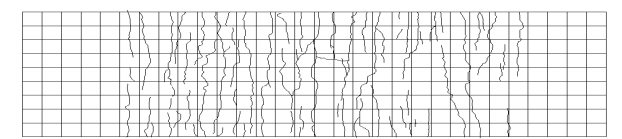
a) YDB-1 side crack



b) YDB-1 bottom crack



c) YDB-2 side crack



d) YDB-2 bottom crack



e) YDB-3 side crack



f) YDB-3 bottom crack

Fig. 6 - Ultimate Failure patterns of RFP slabs.

The elastic phase lasted from the start of the loading to the initiation of cracks on the concrete. In this phase, tensile bar strain, concrete compressive strain, and midspan deflection were relatively small initially. With the increase of load, the values of the three parameters exhibited a linear growth. Thus, the specimens showed obvious features of elastic deformation.

The elastic-plastic stage lasted from the crack initiation on the concrete to the yield of the tensile bars. On all six specimens, the first crack appeared at the pure bending zone at the slab bottom or near the load points at the bending-shear zone. With the increase of load, the crack developed rapidly in both the pure bending zone and the bending-shear zone. After a period of loading, the crack development gradually slowed down: a few parallel main cracks appeared in the pure bending zone, which were evenly distributed and vertical to the axis of the specimen. As the load approximated the yield load, the cracks on the 3

composite slabs continued to propagate, giving off banging noises. Meanwhile, multiple cracks penetrated the slab bottom and several side cracks extended onto the contact area.

The failure phase lasted from the yield of the longitudinal tensile bars at the slab bottom to the ultimate state (i.e. the slab could no longer withstand the load or the crack width/midspan deflection exceeded the specified limit). In this phase, the load increased at a slower pace; the steel fibres of YDB-2, YDB-3, DHB-2 and DHB-3 were pulled out from the tensile zone of the concrete, a few of which were broken; the side cracks extended quickly upwards; the bottom cracks further developed into multiple penetrating cracks; both crack width and slab deflection increased rapidly. In this case, the slab bottom deflection and maximum crack width surpassed the requirements, marking the beginning of the ultimate state (i.e. the failure of the specimen). The three composite slabs were ranked as DHB-3 > DHB-1 > DHB-2 in terms of ultimate strength. As for the three RPF base slabs, several transverse cracks appeared on the surface in the later stage of loading, owing to the thin slab thickness. The cracking was particularly serious on DHB-2: two cracks emerged atop the rectangular fins. Finally, the RPF base slabs failed due to the yield of bottom bars and excess midspan deformation. The three base slabs were ranked as YDB-3 > YDB-1 > YDB-2 in terms of ultimate strength.

3.2. Load-deflection curve

The load-midspan deflection curves of the composite slab specimens are presented in Figure 7, and those of the base slab specimens are shown in Figure 8.

The following trends can be observed from the load-midspan deflection curves in Figures 7 and 8.

1) The load-midspan deflection curves of all six specimens were composed of three segments. Comparatively, the curves of base slab specimens were significantly lower than those of composite slab specimens, because of their thin thickness (60mm) and small second moment of area.

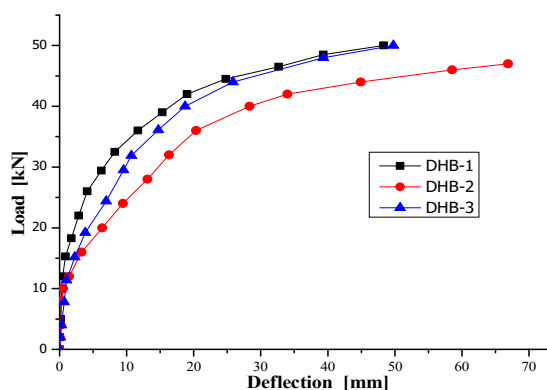


Fig. 7 - Load-midspan deflection curves of composite slabs.

2) Elastic phase: At the beginning, the load was small and the concrete was not cracked. In this case, the load is directly proportional to deflection. This period was rather short due to the weak tensile strength of concrete. The load-midspan deflection curve of each specimen was a short straight line with steep slope.

3) Elastic-plastic phase: As the loading continued, the lower concrete cracked and lost its function. Then, the tensile force was entirely borne by rebars, leading to lower specimen rigidity and faster deflection growth. Before the bar stress reached the yield strength, cracks appeared in the bottom concrete and continued to propagate, the specimens became less and less rigid, and the load-midspan deflection curve gradually flattened out. The rigidity decline was relatively slow in composite slabs DHB-2 and DHB-3 and base slabs YDB-2 and YDB-3, for the crack development, propagation and penetration are suppressed by the bridging effect and high-tensile strain features of steel fibres. In general, the load-midspan deflection curves of DHB-2, 3 and YDB-2, 3 were respectively smoother than that of DHB-1 and YDB-2.

4) Failure phase: When the load reached the yield strength of bars, the positive effects of bars on the specimens were weakened and even eliminated with the pulling out of the bars. Despite the invariance of the load, the specimens were deformed rapidly. With the slow growth of load, the load-midspan deflection curve quickly shifted towards the deflection axis. Compared to composite slabs, the base plates YDB-2 and 3 reveal the poor ductility and low strength of concrete made from recycled aggregates. In their load-midspan deflection curves, the curvature plunged deeply while the deflection soared beyond the specified limit.

5) Comparing the deflections in the same phase, the composite slabs were ranked as DHB-1 > DHB-2 > DHB-3 while the base plates were ranked as YDB-2 > YDB-1 > YDB-3.

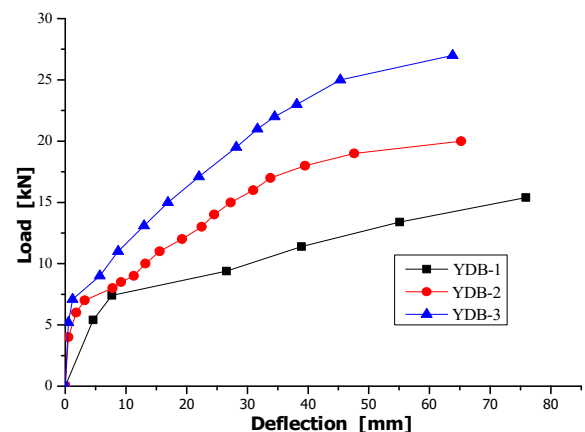


Fig. 8 - Load-midspan deflection curves of base slabs.

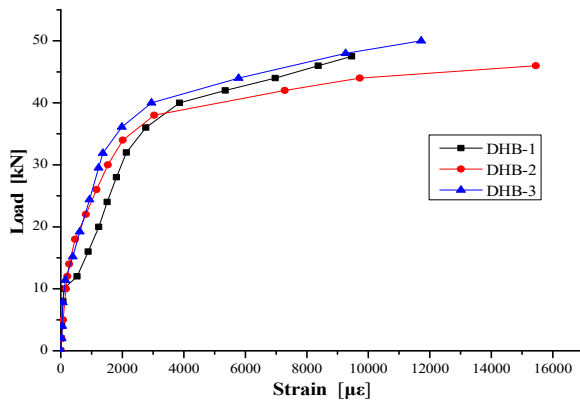


Fig. 9 - Load-midspan bar strain curves of composite slabs.

3.3. Load-bar strain curves

The following trends can be observed from the relationship curves between load and the midspan strain of longitudinal tensile bars at the bottom of slab in Figures 9 and 10.

1) The bar strain curves of all six specimens were composed of three segments: the straight segment before concrete cracking, the curved segment between the cracking and bar yielding, and the smooth segment between bar yielding and the ultimate state.

2) Elastic phase: A similar trend, i.e. linear increase, was observed from the load-midspan bar strain curves of all six specimens.

3) Elastic-plastic phase: Because of the cracking resistance and enhancement effect of steel fibres, the crack propagation was slowed down after the cracking of the concrete. The tensile stress of the cracked concrete was partially borne by these fibres. Unlike the specimens made from ordinary concrete, DHB-2, 3 and YDB-2, 3 had no obvious inflection points on the load-midspan bar strain curves under the same conditions.

4) Failure phase: When the load reached the yield strength of bars, the positive effects of bars on tensile recycled concretes in DHB-2, 3 and YDB-2, 3 were weakened with the pulling out of the bars. In this phase, the bar strain was increased. Compared to specimens made from ordinary concrete, these specimens had smooth load-midspan bar strain curves.

3.4. Synergic effect of old and new concretes

The shear strength and structure of composite bending concrete components are clearly specified in the Code for Design of Concrete Structures (GB50010-2010 (2016)): the surface of a composite slab without stirrups must be roughened to ensure that the convex-concave degree is greater than 4mm and the concrete in the contact area should not be lower than C20 [14]. However, these requirements are targeted at the composition of two ordinary concretes, and may not apply to the composition between recycled concrete and ordinary concrete. Despite many similarities [15-27]

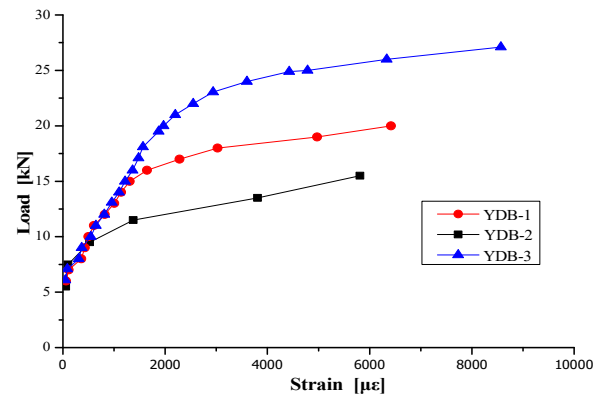


Fig. 10 - Load-midspan bar strain curves of base slabs.

recycled concrete differed from ordinary concrete in structural properties, such as deformation degree and cracking time. The synergic effect of the composite made from recycled concrete and ordinary concrete relies on the bonding property of the contact area.

3.4.1. Contact area

After the completion of loading, all composite specimens were peeled off for analysis. It can be seen from the failure sections that: the fracture faces of recycled concretes mainly concentrated on coarse aggregates; the coarse aggregates at the bottom cracks of DHB-2 were almost entirely broken. By contrast, the fracture faces of DHB-1 appeared mostly at the contact area between mortar and coarse aggregates; only a few of them emerged on coarse aggregates; the fracture faces were smooth and clear.

Throughout the loading process, there was no slippage, break-off or hollowing before the failure of composite slabs, a signal of the good bonding between the base plate and the upper-layer concrete. Thus, the bonding effect between recycled concrete and ordinary concrete and the load-bearing capacity of the composite slabs are not hindered by material differences (e.g. elastic modulus and compressive strength) between the two types of concretes. It is safe to say that the bonding effect of the contact area between recycled concrete and ordinary concrete is similar to that of the contact area between ordinary concretes.

3.4.2. Load-compressive strain curves

Based on the values measured by strain gages at relevant positions, the load-midspan strain curves of concrete at the tensile area at the top of composite slabs and the distribution of concrete strain at different heights of midspan section were plotted as Figures 11 and 12, respectively.

As shown in Figure 11, the load-midspan strain curves of concrete all contained three different stress phases; no concrete was crushed in the tensile area of any specimen; the ultimate compressive strain $\epsilon=0.0033$ was not reached by

any concrete on the top of any specimen. These phenomena demonstrate the excellent bonding and synergic effects between old and new concretes. In the elastic phase, the curves were basically straight lines as the composite slabs were gradually loaded to cracking. From the cracking to failure, the curves gradually stabilized with the increase of the load. This is because the upper-layer concrete gradually exhibited plastic features after the specimens entered the elastic-plastic phase; the neutral axis of concrete section rose rapidly, and the tensile area of the concrete became shorter and shorter.

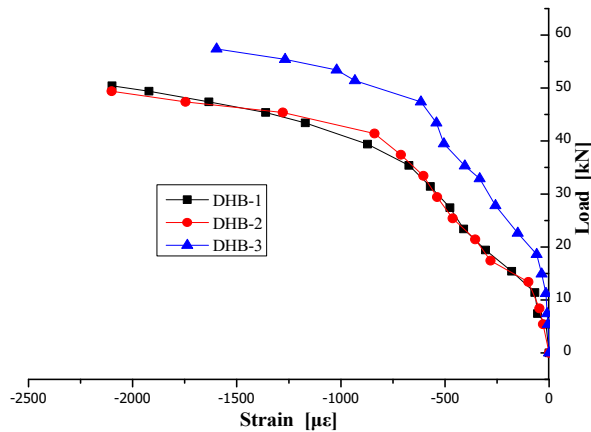
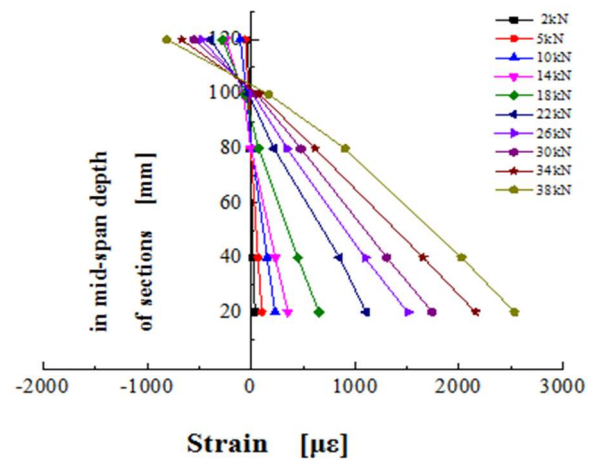


Fig. 11 - Load-midspan strain curves of concrete at the tensile area at the top of composite slabs.

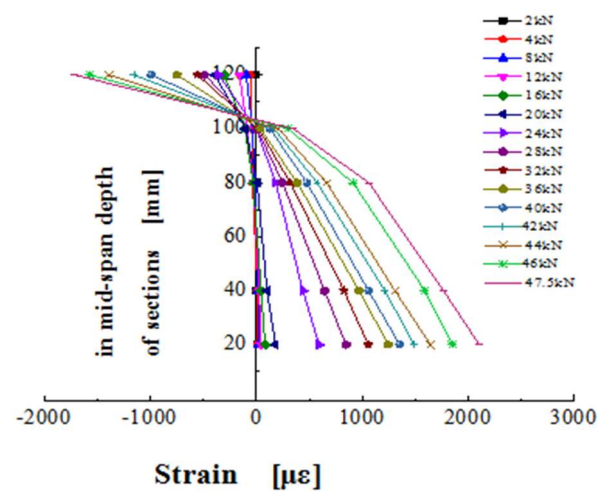
As shown in Figure 12, the midspan strain of concrete basically changed linearly along the section height; with the increase of external load, the neutral axis moved upwards continuously; although the curves show some inflection points, the overall trend remained the same: the strain at each measuring point is positively correlated with the distance from that point to the neutral axis. The bending process of the 3 composite slabs supports the assumption that the plane section remains plane. Under the same conditions, the composite slabs made from fibre-reinforced concrete enjoy the good force-transfer property at the seams and the excellent integrity of those made from ordinary concrete.

3.4.3. Feature parameters

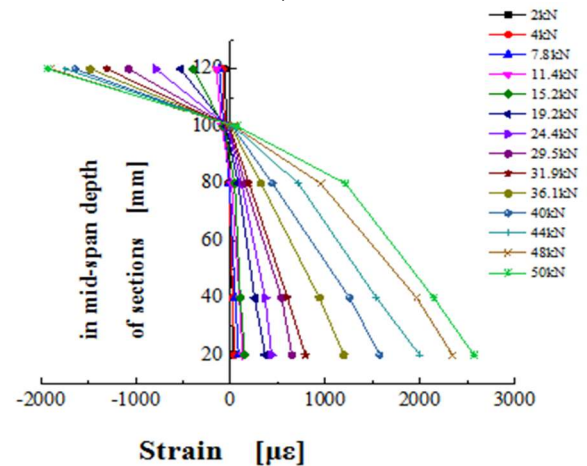
The cracking moment (M_{cr}), ultimate bending moment (M_u), maximum crack width (w_{max}) and the maximum deflection (δ_{max}) (Table 4) of the specimens were compared one by one. It is learned that the composite slabs greatly outperformed the corresponding base plates in both cracking moment and ultimate bending moment, thanks to the improvement of sectional bending rigidity by the pouring of the upper-layer concrete. For instance, DHB-2 surpassed YDB-2 by 63.67% in cracking moment and 208.38% in ultimate bending moment. Meanwhile, the composite slabs had smaller maximum midspan deflection than the corresponding base plates. For example, the



a) DHB-1



b) DHB-2



c) DHB-3

Fig. 12 - Distribution of concrete strain at different heights of midspan section.

maximum midspan deflection of DHB-3 was 28.19% smaller than that of YDB-3. Furthermore, the composite slabs DHB-2, 3 and the base plates YDB-2, 3 had a smaller maximum bottom concrete width than DHB-1 and YDB-1, respectively, because the steel fibres can suppress the cracks.

Table 4

Feature parameters

| No. | Cracking moment /kN·m | Ultimate bending moment /kN·m | Maximum deflection /mm | Maximum crack width /mm |
|-------|-----------------------|-------------------------------|------------------------|-------------------------|
| YDB-1 | 2.99 | 7.24 | 65.20 | 1.00 |
| DHB-1 | 3.84 | 18.18 | 66.90 | 2.00 |
| YDB-2 | 2.78 | 5.61 | 75.89 | 0.50 |
| DHB-2 | 4.55 | 17.30 | 62.03 | 1.80 |
| YDB-3 | 3.34 | 9.37 | 63.8 | 0.70 |
| DHB-3 | 4.33 | 19.24 | 49.77 | 1.60 |

4. Conclusions

Under static vertical load, the base slabs and composite slabs made from recycled concretes shared the same failure process with those made from ordinary concretes, both covering such three periods as elastic phase, elastic-plastic phase and the failure phase. The ultimate failure mode is ductile failure.

Throughout the loading process, no horizontal crack appeared on the contact area of any composite slab; the base plates were bonded well with the upper-layer concretes; in any phase, the mean strain on the normal sections of each composite slab supports the assumption that the plane section remains plane. These phenomena demonstrate the excellent bonding and synergic effects between old and new concretes.

The base plate made from Concrete B boasted the highest bearing capacity and lowest deflection among all base plates and composite plates investigated in our research.

Acknowledgements

This research is made possible thanks to the generous support from National Natural Science Foundation of China (Grant No.: 51578446) and the University Innovation Project Fund of Chinese Ministry of Education (Grant No.: IRT_17R84).

REFERENCES

- X. Lu, Precast concrete structures in the future, *Structural Concrete*, 2014, **15**(1), 1.
- N. Reis, J.D. Brito, J.R. Correia, M. Arruda, Punching behaviour of concrete slabs incorporating coarse recycled concrete aggregates, *Engineering Structure*, 2015, **100**, 238.
- Y.Y. Liu, N. Xiao, F.J. Wen, Study of architectural shading system based on BIPV, *Mathematical Modelling of Engineering Problems*, 2016, **3**(3), 115.
- C.M. Liu, L. Liu, C.B. Liu, Analysis of wind resistance of high-rise building structures based on computational fluid dynamics simulation technology, *International Journal of Heat and Technology*, 2018, **36**(1), 376.
- C.J. Liu, Optimal design of high-rise building wiring based on ant colony optimization, *Cluster Computing*, 2018, **5**, 1.
- V. Bianco, G. Piazza, F. Scarpa, L.A. Tagliafico, Energy, economic and environmental assessment of the utilization of heat pumps for buildings heating in the Italian residential sector, *International Journal of Heat and Technology*, 2017, **35**(S1), S117.
- M. Li, Z. Sun, W. Zhao, Y. Liu, Research Progress on Reinforced Concrete Laminated Slab in China, *Applied Mechanics & Materials*, 2012, 263.
- W. Huang, B. Li, L. Song, Y. Xiong, Orthogonal experiment research on the strength of fiber reinforced silt ceramsite concrete, *Journal of Xi'an University of Architecture & Technology (Natural Science Edition)*, 2017, **49**(1), 22.
- B. Li, W. Huang, C. Li, K. Dong, Study on damage constitutive model of steel fiber recycled brick aggregate concrete, *Journal of Huazhong University of Science and Technology (Natural Science Edition)*, 2017, **45**(1), 17.
- H. Huang, F. Wu, M. Zhu, C. Zeng, W. Lv, Influence of rib details on flexural behavior of concrete composite slab with precast prestressed ribbed panel, *Journal of Building Structures*, 2015, **36**(10), 66.
- H. Huang, F. Wu, W. Chen, X. Zhou, Experimental Study and Calculating Methods on Bending Rigidity of Precast Prestressed Concrete Ribbed Panels for Composite Slabs, *Journal of Hunan University (Natural Sciences)*, 2011, **38**(4), 1.
- H. Liu, Q. Jiang, Experiment of inverted "T" simply supported composite slab, *Journal of Hunan University (Natural Sciences)*, 2004, **35**(1), 147.
- National standards of the CHN. Standard Methods for Testing of Concrete Structures, GB/T 50152-2012, Beijing: China Architecture & Building Press, 2012.
- The industry standard of the CHN. Technical specification for precast concrete walls, JGJ1 2014, Beijing: China Architecture & Building Press, 2014.
- T. Paulay, R. Park, M.H. Phillips, Horizontal construction joints in cast in place reinforced concrete, *Shear in Reinforced Concrete*. 1974, **2**, 599-616.
- D. Dujmović, B. Androić, D. Tonis, I. Lukačević, Composite columns made of concrete-filled hollow steel sections with embedded steel cores, *Technical Gazette*, 2017, **4**(69), 295.
- Z. Bayasi, H. Kaiser, M. Gonzales, Composite slabs with corrugated SIMCON-Deck as alternative for corrugated metal sheets, *Journal of Structural Engineering*, 2001, **127**(10), 1198-1205.
- H.S. Abbas, S.A. Bakar, M. Ahmadi, Z. Haron, Experimental studies on corrugated steel-concrete composite slab, *Gradevinar*, 2015, **67**(3), 225.
- E. Kaszewska, M. Fragiaco, H. Johnsson, Laboratory Tests and Numerical Analyses of Prefabricated Timber-Concrete Composite Floors, *Journal of Structural Engineering*, 2010, **136**(1), 46.
- B.J. Daniel, Composite Slab Behavior and Strength Analysis. Part I: Calculation Procedure, *Journal of Structural Engineering*, 1993 **119**(1), 16.
- M. Rakočević, Stress in multilayered composite slabs, *Gradevinar*, 2005, **57**(7), 503.
- C. Hector, M. Fernando, Experimental study on shear bond behaviour of composite slabs according to Eurocode 4, *Journal of construction steel research*, 2013, **82**(3), 99-110.
- Dai, Y.; Zhu, X.; Chen, L.S. A MECHANICAL-HYDRAULIC VIRTUAL PROTOTYPE CO-SIMULATION MODEL FOR A SEABED REMOTELY OPERATED VEHICLE. *International Journal of Simulation Modelling*, 2016, **15**(3): 532.
- M. Ferrer, F. Marimon, M. Crisinel, Designing cold-formed steel sheets for composite slabs: An experimentally validated FEM approach to slip failure mechanics, *Thin-Walled Structures*, 2006, **44**(12), 1261.
- W. Huang, M. Zhang, H. Meng, C. Zhang, Study on seismic behavior of ecological composite walls filled with different materials, *Journal of Investigative Medicine*, 2014, **62**(8), 51.
- S. Ravai Nagy, M. Lobonțiu, Gear teeth bending test upon the gear with asymmetric teeth, *Academic Journal of Manufacturing Engineering*, 2015, **13**(1), 63.
- Y. Dai, L. S. Chen, X. Zhu, H. Liu, Modelling and simulation of a mining machine excavating seabed massive sulfide deposits. *International Journal of Simulation Modelling*, 2016, **15**(2), 377.
